Local Order and Rotational Dynamics in Mixed A-Cation Lead Iodide Perovskites

Giuseppe Fisicaro, Antonino La Magna, Alessandra Alberti, Emanuele Smecca, Giovanni Mannino, and Ioannis Deretzis*

Istituto per la Microelettronica e Microsistemi (CNR-IMM), Z.I. VIII strada 5, 95121 Catania, Italy

E-mail: ioannis.deretzis@imm.cnr.it

Abstract

Halide perovskites containing a mixture of formamidinium (FA^+), methylammonium (MA^+) and cesium (Cs^+) cations are the actual standard for obtaining record-efficiency perovskite solar cells. Although the compositional tuning that brings to optimal performance of the devices has been largely established, little is understood on the role of even small quantities of MA^+ or Cs^+ in stabilizing the black phase of $FAPbI_3$ while boosting its photovoltaic yield. In this paper, we use Car-Parrinello molecular dynamics in large supercells containing different ratios of FA^+ and either MA^+ or Cs^+, in order to study the structural and kinetic features of mixed perovskites at room temperature. Our analysis evidences that cation mixing relaxes the rotational disorder of FA^+ molecules by preferentially aligning their axis towards $\langle 1\,0\,0 \rangle$ cubic directions. The phenomenon stems from the introduction of additional local minima in the energetic landscape, which are absent in pure $FAPbI_3$ crystals. As a result, a higher structural order is achieved, characterized by a pronounced octahedral tilting and a lower vibrational activity for the inorganic framework. We show that both MA^+ and Cs^+ are qualified for this enhancement, with Cs^+ being particularly effective when diluted within the $FAPbI_3$ perovskite.

Graphical TOC Entry

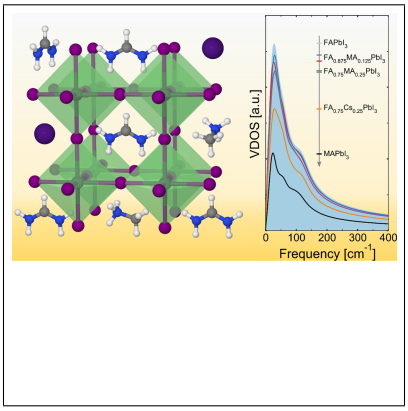

Hybrid halide perovskites have reached their first decade as an emerging photovoltaics technology[1] and the interest on their exceptional photosensitizing properties is being constantly sustained by new efficiency records in single-junction or tandem solar cells.[2] The quest for more stable and performing materials has gradually driven research from methylammonium lead iodide ($MAPbI_3$) towards mixed perovskites,[3,4] where formamidinium (FA^+), methylammonium (MA^+) and cesium (Cs^+) ions alternate in the occupation of the A-sites, i.e. the cubic cavities of the octahedral ABX_3 perovskite structure. The principal evolution strategy has promoted the substitution of MA^+ with FA^+, as the latter proved to be thermally more stable.[5,6] Pure α-$FAPbI_3$ has similar electronic characteristics as $MAPbI_3$ close to the valence and conduction band edges.[7] However, its spontaneous tendency to form a non-perovskite δ-phase at room temperature[8,9] complicates its use in photovoltaics. The introduction of Cs^+ within the $FAPbI_3$ lattice (i.e. the partial substitution of FA^+ with Cs^+) can largely retard the transformation of the black perovskite phase into the inactive yellow phase of $FAPbI_3$.[10,11] The further addition of MA^+ as a second minority cation can bring to record-high photovoltaic efficiencies,[12] making triple A-cation mixtures a very common system for perovskite solar cells. The enhanced perovskite stability with mixed A-cations has been previously attributed to a lowering of the Gibbs free energy by increasing the entropy,[10] or to refinements in the Goldschmidt tolerance factor.[13,14] However, the atomic-level understanding of the dynamic features that take place when MA^+/Cs^+ are present in a $FAPbI_3$ crystal is still unclear. This aspect is essential for engineering optimized hybrid materials, or even for totally moving towards organic-free structures.[15]

The pivotal role of MA^+ and Cs^+ as minority cations in making highly efficient and stable $FAPbI_3$-based perovskite solar cells is therefore something that requires further investigation. Electronically, FA^+, MA^+ and Cs^+ introduce energy levels that are too far away from the perovskite band gap states, formed by antibonding $I-5p$, $Pb-6s$ and $Pb-6p$ orbitals.[16] Hence, A-cations do not actively take part in the photogeneration process. However, the type of A-cation can indirectly impact on the bandgap value through the tilting of the $[PbI_6^{4-}]$

octahedra, or by variation of the lattice constants.[17] It has been experimentally observed that the value of the bandgap is smaller in $FAPbI_3$ with respect to $MAPbI_3$ or $CsPbI_3$.[18,19] This aspect indicates that the introduction of MA^+/Cs^+ in $FAPbI_3$ can hardly explain an enhancement in the photoabsorption. Ghosh *et al.* have theoretically argued that the inclusion of Cs^+ could give rise to a direct-to-indirect band gap transition through Rashba-type effects that could reduce the rate of carrier recombination.[20] It is also possible though that similar events could lower the rate of photogeneration. Finally, a room-temperature tetragonal phase (which could favor the photovoltaic effect[21]) is absent in mixed perovskites, where the cubic phase of $FAPbI_3$ prevails.[13] All the above issues suggest that the efficiency improvements in mixed Cs^+-FA^+-MA^+ perovskite systems are difficult to be explained solely through the electronic, optical or polarization properties of the perovskite material.

It is useful to consider here that the photovoltaic effect is not simply a charge generation but also a charge transport phenomenon, where the photogenerated carriers must travel towards the electron and hole transporting layers prior to being collected by the electrodes. Charge generation is largely influenced by the electronic/optical properties of the material whereas charge transport, in addition to intrinsic lattice characteristics (e.g. effective mass), can be also influenced by the dynamic properties of the lattice (e.g. phonons, defects, etc.). Intrinsically, the presence of cations with different structural and vibrational features can alter the dynamic properties of the entire perovskite layer. It becomes therefore interesting to investigate if vibrational issues can influence the photovoltaic response.

Having this aspect in mind, in this paper we use a number of static (density functional theory, nudged elastic band) and dynamic (Car-Parrinello molecular dynamics) *ab initio* computational techniques to study the role of minority fractions of MA^+ or Cs^+ in an otherwise ideal $FAPbI_3$ crystal. We particularly focus on the molecular dynamics approach that has been widely used in the perovskite literature,[22–31] as it is able to capture the anharmonic nature of the atomic vibrations in hybrid perovskite crystals.[32] We show that MA^+ and Cs^+ introduce additional local minima in the energy landscape of the perovskite

and induce local ordering features that impact on the vibrational properties of the entire system. As a result, the mixed perovskite is characterized by an inorganic framework with lower vibrational intensity than $FAPbI_3$, which is a feature that should facilitate the excitonic transport towards the electron and hole transporting layers.

The three A-cations considered in this study present different geometric and polarization features (Fig. 1). MA^+ is an sp^3-hybridized polar cation with a positive charge mainly localized towards its -NH_3 moiety. FA^+ is an sp^2 cation that also preserves a polar character but with a significantly smaller dipole moment.[33] Its positive charge is delocalized between the two -NH_2 groups of the molecule and as a consequence, its polar axis is perpendicular to the axis crossing these groups. On the contrary, Cs^+, as a single-atom cation, does not have a polar character. The dimensions of the three cations can be approximately estimated by their center of mass and ionic radii.[34] Based on this scheme, FA^+ is bigger than MA^+ and Cs^+. The respective lead iodide perovskites (Fig. 1a-c) form different crystallographic phases at room temperature: $MAPbI_3$ is tetragonal[6,35] (stable), $FAPbI_3$ is cubic[13] (unstable) and $CsPbI_3$ is orthorhombic[36] (unstable). Such divergences raise questions on the role of mixing A-cations in the structural or vibrational properties of the perovskite system.

In order to investigate this issue we have performed the following computational experiments: We have set up Car-Parrinello[37] molecular dynamics simulations for systems comprising $4 \times 4 \times 2$ cubic supercells, for a pure $FAPbI_3$ crystal as well as for $FA_{1-x}MA_xPbI_3$ mixed perovskites containing a concentration of either 12.5% or 25% of MA^+ cations. For

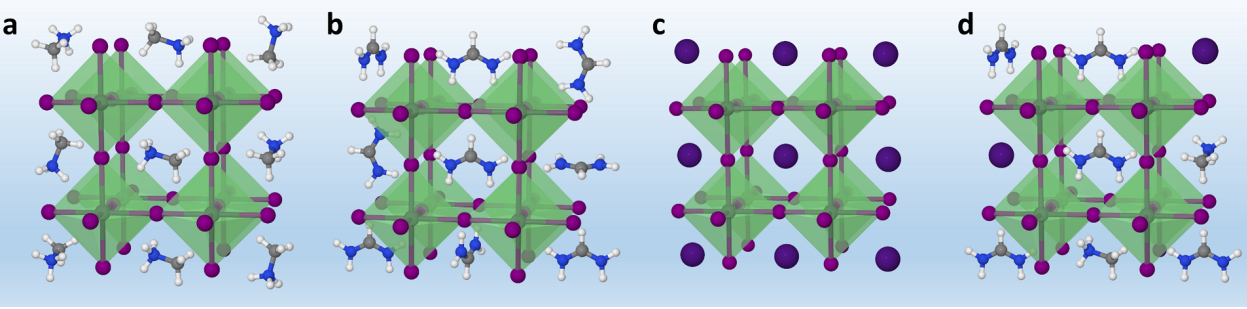

Figure 1: Schematic representation of (a) $MAPbI_3$, (b) $FAPbI_3$, (c) $CsPbI_3$ and (d) mixed $Cs_xMA_yFA_{1-(x+y)}PbI_3$ perovskites.

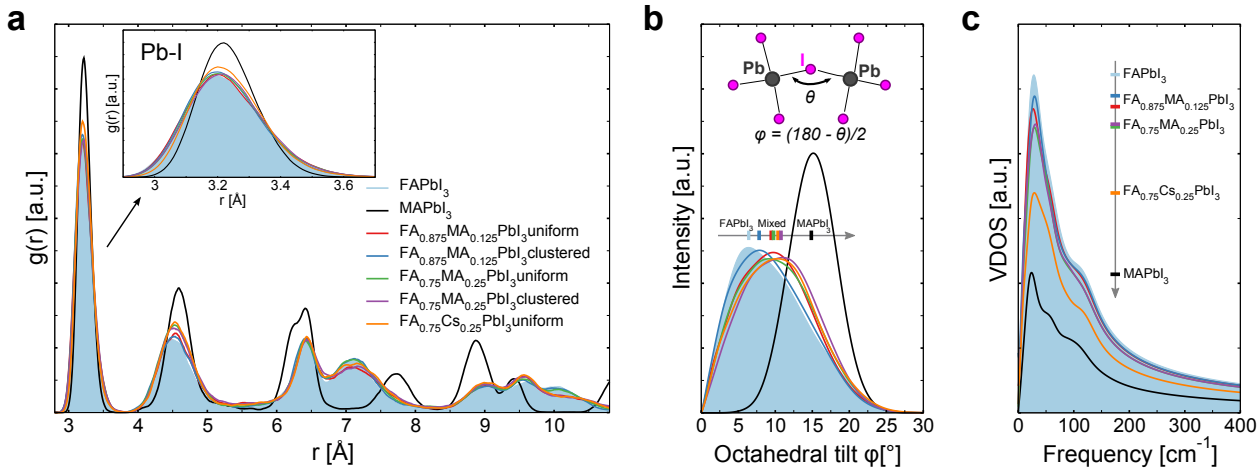

Figure 2: (a) Radial distribution function calculated for $FAPbI_3$ (shaded light-blue area), $MAPbI_3$ (black line), $FA_{0.875}MA_{0.125}PbI_3$ (red for uniform and blue for clustered configurations), $FA_{0.75}MA_{0.25}PbI_3$ (green for uniform and violet for clustered configurations) and $FA_{0.75}Cs_{0.25}PbI_3$ (orange line). (b) Octahedral tilting angle ϕ for pure and mixed perovskites. (c) Vibrational density of states of the Pb-I inorganic framework for pure and mixed perovskites. All quantities refer to perovskite structures at room temperature. The color schemes are common for all figures.

the mixed systems, we further considered two configurations where the minority cations were either uniformly distributed within the $FAPbI_3$ matrix or aggregated at a corner of our computational box (see Fig. S1). We repeated a similar calculation in the case of 25% of uniformly distributed Cs^+ ($FA_{0.75}Cs_{0.25}PbI_3$). The equations of motion were followed for 40 ps, apart from the $FA_{0.75}Cs_{0.25}PbI_3$ perovskite, where 20 ps were enough for reaching the thermodynamic equilibrium. The last 10 ps of the calculations were used in order to extrapolate the statistical properties. The $MAPbI_3$ perovskite was also considered as a reference system.[24,32] All calculations took place at room temperature.

We first compared the radial distribution function of the inorganic bonds for all perovskites (Fig. 2a). Qualitative differences were present only for the $MAPbI_3$ system (especially for distances greater than 6 Å), as this crystallizes in the tetragonal phase at room temperature, whereas all other perovskites ($FAPbI_3$ and mixed) maintain a cubic arrangement. The first peak of the radial distribution function corresponds to the statistical distribution of the Pb-I bonds (Fig. 2a-inset). Here, smaller bond fluctuations are observed for

the tetragonal $MAPbI_3$ with respect to the other systems. A closer examination of this peak shows that also the $FA_{0.75}Cs_{0.25}PbI_3$ perovskite narrows the Pb-I bond variability. In the literature, either $MAPbI_3$ or mixed perovskites containing Cs^+ are considered as the most stable at room temperature.[6,10] We therefore note a correlation between the statistical Pb-I bond-length fluctuations and the stability of the perovskite system. As a further structural benchmark, we calculated the tilting angles ϕ between nearby $[PbI_6^{4-}]$ octahedra, defined as $\phi = (180° - \theta)/2$, where θ is the angle centered on I atoms connecting two neighboring octahedra (Fig. 2b). A clear trend towards higher values of ϕ was observed for the mixed systems, which was quantitatively proportional to the concentration of the minority MA^+ or Cs^+ cations. The ϕ values for $MAPbI_3$ were the highest, as octahedra are always titled in the tetragonal phase. Tilting can be associated with the bandgap of a perovskite system, where a higher angle ϕ corresponds to higher bandgap value.[17] With this respect, the results of Fig. 2b can be viewed as a tendency of mixed systems to slightly increase the bandgap of the $FAPbI_3$ perovskite. This is a factor that can positively influence the open-circuit voltage while negatively impact on the short-circuit current of the solar cells. Out of all studied systems, the $MAPbI_3$ perovskite should have the highest bandgap at room temperature, which is consistent with the experimental literature.[18] Lastly, in order to investigate how bond lengths and tilting angles can influence the vibrational properties of the perovskite systems, we calculated the vibrational intensity as a function of the phonon frequency through a Fourier transform of the velocity autocorrelation function (Fig. 2c). Results showed that the introduction of MA^+ or Cs^+ in the $FAPbI_3$ crystal should lower the vibrational density of states (VDOS) of the perovskite system according to the following guidelines: (a) higher concentrations of the minority A-site cations (25% here) should decrease the VDOS more than lower concentrations (12.5% here), (b) a homogeneous dilution of the A-cations should decrease the VDOS more than a non-homogeneous dilution and (c) upon equal concentrations and local configuration, the Cs^+ cation should be significantly more effective in reducing the VDOS with respect to MA^+. We note that the lowest VDOS

for all the studied systems is achieved by the tetragonal $MAPbI_3$ perovskite, in accordance with the smaller fluctuations of its Pb-I bonds. With this respect, the $MAPbI_3$ lattice should be characterized by the most robust inorganic framework among all studied systems, having though the most unstable A-cation.[5,38] We finally point out that clustered cations should have a lower impact on the vibrational properties of mixed perovskites, indicating that an efficient and homogeneous dilution of the A-cationic species is fundamental for obtaining high-quality perovskite solar cells.

The results of the statistical analysis for the pure and mixed systems can be summarized as follows: Cation mixing tends to reduce the inorganic bond-length fluctuations and increase the tilting angles between nearby $[PbI_6^{4-}]$ octahedra, which impact on the vibrational properties of the system by lowering the phonon intensity of the inorganic framework. Considering that the photogenerated carriers travel on the $[PbI_6^{4-}]$ network prior to being collected by the transporting layers, it appears that cation mixing should facilitate charge transport and consequently raise the probability of successful electron/hole collection. As the only microscopic change between a pure $FAPbI_3$ crystal and the mixed perovskite lies in the composition of the A-cations, we asked which are the local mechanisms that lead to such structural modification. We consequently monitored the local changes in the rotational dynamics of the FA^+ (majority) cations in the case of the presence or absence of MA^+ and Cs^+ (minority cations) within the perovskite crystal. We initially traced the orientations of the FA^+ dipole moments during the molecular dynamics simulation and observed that these should be quasi-randomly distributed towards all directions for both pure and mixed systems (Fig. S2 and S4). We noticed though a more confined rotational distribution when minority cations were present within the computational cell that excluded the corners of the cubic inorganic cage. The absence of preferential orientations for the molecular dipoles in both mixed perovskites and $FAPbI_3$ indicates that such materials should not be ferroelectric at room temperature. This aspect is in contrast with $MAPbI_3$, where room-temperature ferroelectricity has been experimentally observed[39–41] and theoretically evaluated.[42]

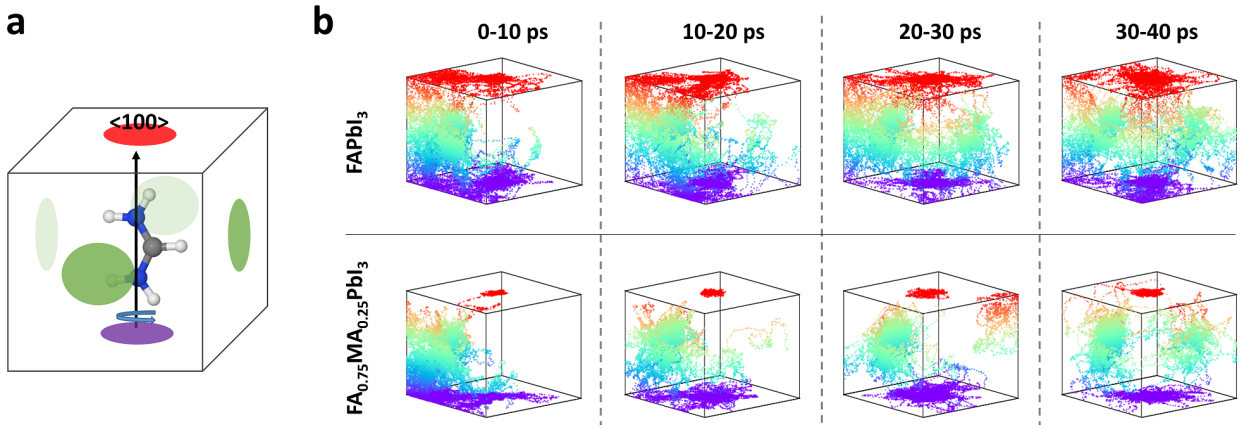

Figure 3: (a) Schematic representation of the preferential orientation of the N-N axis of FA^+ pointing towards $\langle 1\,0\,0 \rangle$ cubic directions in mixed A-cation perovskite systems. (b) Projection of the N-N axis of the FA^+ ions on the cubic inorganic framework for every 10 *ps* of simulation time, for the $FAPbI_3$ system and the $FA_{0.75}MA_{0.25}PbI_3$ system having a clustered MA^+ configuration. The colorscale refers to the z-coordinate of the projections and is used as a guide for the eye.

The qualitative differences in the rotational distribution of the FA^+ molecular dipoles when MA^+ or Cs^+ were present in the perovskite crystal, motivated us to further investigate the manifestation of local ordering features that could explain the macroscopic statistical quantities of Fig. 2. We thereon considered the orientation of the axis passing through the two nitrogen atoms of the formamidinium molecule (Fig. 3a) and performed the same type of analysis (N-N axis from now on). In this case we observed that the orientation of the N-N axis maintained quasi-random positions only for the $FAPbI_3$ perovskite, while it gradually obtained preferential positions towards all $\langle 1\,0\,0 \rangle$ directions of the cubic cavity for mixed perovskites (Fig. 3b). In agreement with the statistical quantities, the concentration and local configuration of the minority cations was important for the manifestation of this effect (see Fig. S3 and S4). We concluded that the enhancement of the structural properties of mixed perovskites has an ordering nature that involves the N-N axis of the FA^+ cations (as also argued in Ref. 20). We note that the confined movement of the FA^+ dipoles discussed above follows the primary ordering effect of the N-N axis. As this is the molecular part where the positive charge is delocalized, we questioned the role of electrostatic interactions in the

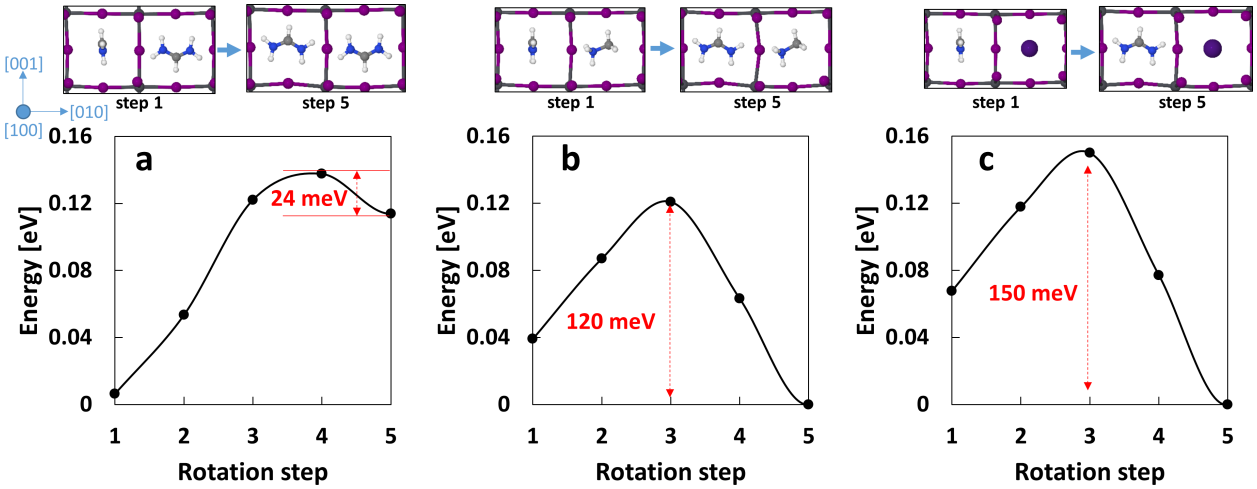

Figure 4: Nudged elastic band calculations for the 90° rotation of an FA^+ cation in (a) $FAPbI_3$, (b) $FA_{0.875}MA_{0.125}PbI_3$ and (c) $FA_{0.875}Cs_{0.125}PbI_3$.

manifestation of this ordering process (or similarly, in the manifestation of the random FA^+ orientations in pure $FAPbI_3$ crystals).

We have examined this issue by performing nudged elastic band calculations in order to calculate the energy barriers and local minima of FA^+ molecules when rotating within the inorganic framework. We considered three cases where an FA^+ cation is rotating in the vicinity of another FA^+ cation (Fig. 4a), an MA^+ cation (within a $FA_{0.875}MA_{0.125}PbI_3$ crystal, Fig. 4b), or a Cs^+ cation (within a $FA_{0.875}Cs_{0.125}PbI_3$ crystal, Fig. 4c). A 90° rotation of FA^+ was considered with its N-N axis transiting from the [1 0 0] to the [0 1 0] direction. In the first case (Fig. 4a) we observed that the rotation path shows only one deep local minimum at the starting configuration, i.e. when the N-N axes of the two neighboring FA^+ cations are perpendicular. The 90° rotation gradually raises the system's energy, while the final configuration (where the N-N axes are parallel) represents a shallow local minimum. This is separated from the transition state by less than 25 meV, indicating that the energetic barrier for escaping from this configuration is smaller than k_BT at room temperature (with k_B the Boltzmann constant). This aspect is important, as it implies that the configuration where two nearby FA^+ cations have parallel N-N axes is highly unstable, as the local interaction between their positive charges becomes non-negligible. At this point the system could simply

return to the initial configuration or find another low-energy local minimum where the N-N axes no longer point towards $\langle 1\,0\,0 \rangle$ directions (Fig. S5), giving rise to the rotational disorder of the $FAPbI_3$ crystal. When the FA^+ ion has a nearby MA^+ instead (Fig. 4b), we observe that the parallel configuration for the N-N axis of the FA^+ and the C-N axis of the MA^+ represents a clear local minimum, while the energetic barrier for escaping from this configuration increases to 120 meV. Finally, when the FA^+ cation has Cs^+ as a nearest neighbor, the configuration where the N-N axis of the FA^+ points towards the Cs^+ ion (step 5) becomes a deep local minimum with an energy barrier of 150 meV separating steps 5 and 1. Considering that the escape frequencies ν from the local minima of step 5 should be compliant with the transition state theory $\nu = \nu_0 \times exp(-E_b/k_BT)$, where E_b is the energy barrier calculated from the nudged elastic band method and ν_0 is the frequency prefactor, we find that escape rates from the local minimum of step 5 should be $\sim$40 times lower when the FA^+ has a nearby MA^+ and $\sim$130 times lower when it has a Cs^+ cation as a neighbour. Hence, the presence of Cs^+ or MA^+ should relax the rotational disorder of FA^+ by reducing the frequencies of rotating events and by preferentially aligning FA^+ cations towards face-centered directions (i.e. $\langle 1\,0\,0 \rangle$), in agreement with the results of the molecular dynamics simulations. A critical point that requires discussion is why triple cation systems show better performances than double FA^+-Cs^+ systems, considering that Cs^+ introduces stronger local minima than MA^+ in the potential energy surface of the mixed perovskites. Our calculations show that the concentration of the minority cations has to be relatively high in order to lower the rotational disorder of the FA^+ ions (25% more than 12.5% here). As high concentrations of Cs^+ are likely to generate aggregated areas within the mixed perovskite system that could lead to the formation of the orthorhombic yellow phase of $CsPbI_3$,[11] the contemporary presence of both MA^+ and Cs^+ should mediate this issue.

In conclusion, our computational findings for mixed FA^+-MA^+ and FA^+-Cs^+ perovkites have evidenced that the principal mechanism for their enhanced stability and photovoltaic response lies in the lower rotational frequencies of the FA^+ cations though a preferential

orientation of their N-N axis towards $\langle 1\,0\,0 \rangle$ directions. Such structural optimization leads to a reduced vibrational activity for the inorganic Pb-I framework, which represents the perovskite sublattice where photogenerated carries travel prior to being collected by the electron and hole transporting layers. Our results have also evidenced that, contrary to the $MAPbI_3$ system, mixed perovskites are unlikely to manifest macroscopic polarization effects at room temperature. Finally, we point out that strategies for the stabilization of lead iodide perovskites should mainly point towards the strengthening of the inorganic framework through the limitation of the bond-length fluctuations for the lead-halogen bonds during the thermal movement of the atoms. This could be achieved with a systematic exploration on partial substitutions of A-cationic species with atoms, molecules or small clusters that could increase the ordering status of the perovskite crystal.

Computational Methods. Calculations were based on various theoretical models of the Quantum Espresso software suite,[43] including Car-Parrinello[37] molecular dynamics (CPMD), density functional theory (DFT) and the nudged elastic band (NEB) method. Molecular dynamics simulations were carried out for $FA_{1-x}MA_xPbI_3$ systems comprising 384 atoms ($4 \times 4 \times 2$ cubic supercells) with a variable concentration (x=0.125 and 0.25) and solubility of the MA^+ cations (uniformly distributed or aggregated). The equations of motion were followed for a total time of 40 ps with a time step of $\sim$0.1 fs. Simulations were performed in the canonical ensemble, setting the target temperature with a Nose thermostat[44] to $T =$ 300 K. The last 10 ps of the calculations were used in order to extrapolate the structural properties of the studied systems in thermodynamic equilibrium. In the case of Cs^+, the uniform $FA_{0.75}Cs_{0.25}PbI_3$ system was considered with 320 atoms, whereas simulation times were restrained to 20 ps due to a faster convergence towards equilibrium. Computations for mixed systems were compared with similar calculations for $FAPbI_3$ and $MAPbI_3$, which were used as a reference. The lattice vector for the cubic systems was set to **a**=6.36 Å, whereas for the tetragonal $MAPbI_3$ we set **a**=**b**=8.86 Å and **c**=12.74 Å. We used the Perdew-Burke-

Ezernhof implementation[45] of the generalized gradient approximation for the description of the exchange-correlation functional. Ultrasoft pseudopotentials[46] were considered for the core electrons, with the exception of the 5d semicore electrons of Pb that were included in the valence group. The cutoff for the kinetic energy and the augmented charge density were set to 35 Ry and 280 Ry, respectively. The Verlet algorithm[47] was employed for the integration of the equations of motion with a time step dt=4 a.u. ($\sim$ 0.1 fs) in order to minimize round-off and truncation errors. All atoms were allowed to move without constraints. The effective electronic mass was assigned to 100 a.u., whereas ionic masses were set to real values. The pair correlation functions $g(r)$ were calculated as

$$\rho g(r) = \frac{1}{N}\left\langle \sum_{i=1}^{N} \sum_{j=1(\neq i)}^{N} \delta(r - r_{ij}) \right\rangle, \tag{1}$$

where ρ is the atomic density, N the total number of atoms within the simulation box and r_{ij} the distance between atomic pairs. The statistical geometrical properties were computed only for the directions of maximum expansion of the supercells (x, y) in order to avoid quantitative errors due to the reduced periodicity of the z direction. The vibrational density of states (VDOS) was computed by squaring the Fourier transform of the velocity autocorrelation function as:

$$VDOS(\omega) = \left| \int \langle \vec{v}(0) \cdot \vec{v}(t) \rangle e^{-i\omega t} dt \right|^2, \tag{2}$$

where ω is the frequency and dt is the time step of the molecular dynamics run.

The climbing-image nudged elastic band method[48] was used to find the transition states of the rotation paths for the formamidinium ions. For these calculations we considered $2 \times 2 \times 2$ cubic supercells. Convergence was achieved through a $4 \times 4 \times 4$ Brillouin zone sampling within the Monkhorst-Pack scheme.[49] DFT and CPMD calculations shared exchange-correlation functionals, pseudopotentials and cutoff parameters.

Acknowledgement

The authors would like to acknowledge the Italian ministry of education and research within the project BEST-4U (CUP B88D19000160005) and the bilateral project between CNR-Italy and JSPS-Japan (CUP B56C18001070005) for partial financial support. Computer resources were provided by the Swiss National Supercomputing Centre (CSCS) under Project ID s869 and the Italian Cineca Consortium under the ISCRA project HYPERSOL (Ref. n. HP10BRZPQ8).

Supporting Information Available

Initial configurations for the CPMD calculations, orientations of the dipole moments and N-N axes of FA^+ cations for pure and mixed systems, density functional theory calculations.

References

(1) Kojima, A.; Teshima, K.; Shirai, Y.; Miyasaka, T. Organometal Halide Perovskites as Visible-Light Sensitizers for Photovoltaic Cells. *J. Am. Chem. Soc.* **2009**, *131*, 6050–6051.

(2) Green, M. A.; Dunlop, E. D.; Hohl-Ebinger, J.; Yoshita, M.; Kopidakis, N.; Ho-Baillie, A. W. Solar Cell Efficiency Tables (Version 55). *Prog Photovolt Res Appl.* **2020**, *28*, 3–15.

(3) Bi, D.; Tress, W.; Dar, M. I.; Gao, P.; Luo, J.; Renevier, C.; Schenk, K.; Abate, A.; Giordano, F.; Baena, J.-P. C. et al. Efficient Luminescent Solar Cells Based on Tailored Mixed-Cation Perovskites. *Sci. Adv.* **2016**, *2*, e1501170.

(4) McMeekin, D. P.; Sadoughi, G.; Rehman, W.; Eperon, G. E.; Saliba, M.; Hörantner, M. T.; Haghighirad, A.; Sakai, N.; Korte, L.; Rech, B. et al. A Mixed-

Cation Lead Mixed-Halide Perovskite Absorber for Tandem Solar Cells. *Science* **2016**, *351*, 151–155.

(5) Smecca, E.; Numata, Y.; Deretzis, I.; Pellegrino, G.; Boninelli, S.; Miyasaka, T.; La Magna, A.; Alberti, A. Stability of Solution-Processed $MAPbI_3$ and $FAPbI_3$ Layers. *Phys. Chem. Chem. Phys.* **2016**, *18*, 13413–13422.

(6) Deretzis, I.; Smecca, E.; Mannino, G.; La Magna, A.; Miyasaka, T.; Alberti, A. Stability and Degradation in Hybrid Perovskites: Is the Glass Half-Empty or Half-Full? *J. Phys. Chem. Lett.* **2018**, *9*, 3000–3007.

(7) Amat, A.; Mosconi, E.; Ronca, E.; Quarti, C.; Umari, P.; Nazeeruddin, M. K.; Gratzel, M.; De Angelis, F. Cation-Induced Band-Gap Tuning in Organohalide Perovskites: Interplay of Spin–Orbit Coupling and Octahedra Tilting. *Nano Lett.* **2014**, *14*, 3608–3616.

(8) Han, Q.; Bae, S.-H.; Sun, P.; Hsieh, Y.-T.; Yang, Y.; Rim, Y. S.; Zhao, H.; Chen, Q.; Shi, W.; Li, G. et al. Single Crystal Formamidinium Lead Iodide ($FAPbI_3$): Insight into the Structural, Optical, and Electrical Properties. *Adv. Mater.* **2016**, *28*, 2253–2258.

(9) Gratia, P.; Zimmermann, I.; Schouwink, P.; Yum, J.-H.; Audinot, J.-N.; Sivula, K.; Wirtz, T.; Nazeeruddin, M. K. The Many Faces of Mixed Ion Perovskites: Unraveling and Understanding the Crystallization Process. *ACS Energy Lett.* **2017**, *2*, 2686–2693.

(10) Yi, C.; Luo, J.; Meloni, S.; Boziki, A.; Ashari-Astani, N.; Grätzel, C.; Zakeeruddin, S. M.; Röthlisberger, U.; Grätzel, M. Entropic Stabilization of Mixed A-Cation ABX_3 Metal Halide Perovskites for High Performance Perovskite Solar Cells. *Energy Environ. Sci.* **2016**, *9*, 656–662.

(11) Schelhas, L. T.; Li, Z.; Christians, J. A.; Goyal, A.; Kairys, P.; Harvey, S. P.; Kim, D. H.; Stone, K. H.; Luther, J. M.; Zhu, K. et al. Insights into Operational Stability and

Processing of Halide Perovskite Active Layers. *Energy Environ. Sci.* **2019**, *12*, 1341–1348.

(12) Holzhey, P.; Yadav, P.; Turren-Cruz, S.-H.; Ummadisingu, A.; Grätzel, M.; Hagfeldt, A.; Saliba, M. A Chain Is as Strong as its Weakest Link–Stability Study of $MAPbI_3$ under Light and Temperature. *Mater. Today* **2019**, *29*, 10–19.

(13) Xie, L.-Q.; Chen, L.; Nan, Z.-A.; Lin, H.-X.; Wang, T.; Zhan, D.-P.; Yan, J.-W.; Mao, B.-W.; Tian, Z.-Q. Understanding the Cubic Phase Stabilization and Crystallization Kinetics in Mixed Cations and Halides Perovskite Single Crystals. *J. Am. Chem. Soc.* **2017**, *139*, 3320–3323.

(14) Li, Z.; Yang, M.; Park, J.-S.; Wei, S.-H.; Berry, J. J.; Zhu, K. Stabilizing Perovskite Structures by Tuning Tolerance Factor: Formation of Formamidinium and Cesium Lead Iodide Solid-State Alloys. *Chem. Mater.* **2015**, *28*, 284–292.

(15) Miyasaka, T.; Kulkarni, A.; Kim, G. M.; Öz, S.; Jena, A. K. Perovskite Solar Cells: Can We Go Organic-Free, Lead-Free, and Dopant-Free? *Adv. Energy Mater.* 1902500.

(16) Shirayama, M.; Kadowaki, H.; Miyadera, T.; Sugita, T.; Tamakoshi, M.; Kato, M.; Fujiseki, T.; Murata, D.; Hara, S.; Murakami, T. N. et al. Optical Transitions in Hybrid Perovskite Solar Cells: Ellipsometry, Density Functional Theory, and Quantum Efficiency Analyses for $CH_3NH_3PbI_3$. *Phys. Rev. Appl.* **2016**, *5*, 014012.

(17) Prasanna, R.; Gold-Parker, A.; Leijtens, T.; Conings, B.; Babayigit, A.; Boyen, H.-G.; Toney, M. F.; McGehee, M. D. Band Gap Tuning via Lattice Contraction and Octahedral Tilting in Perovskite Materials for Photovoltaics. *J. Am. Chem. Soc.* **2017**, *139*, 11117–11124.

(18) Jacobsson, T. J.; Correa-Baena, J.-P.; Pazoki, M.; Saliba, M.; Schenk, K.; Grätzel, M.; Hagfeldt, A. Exploration of the Compositional Space for Mixed Lead Halogen Perovskites for High Efficiency Solar Cells. *Energy Environ. Sci.* **2016**, *9*, 1706–1724.

(19) Eperon, G. E.; Paterno, G. M.; Sutton, R. J.; Zampetti, A.; Haghighirad, A. A.; Cacialli, F.; Snaith, H. J. Inorganic Caesium Lead Iodide Perovskite Solar Cells. *J. Mater. Chem. A* **2015**, *3*, 19688–19695.

(20) Ghosh, D.; Smith, A. R.; Walker, A. B.; Islam, M. S. Mixed A-Cation Perovskites for Solar Cells: Atomic-Scale Insights into Structural Distortion, Hydrogen Bonding, and Electronic Properties. *Chem. Mater.* **2018**, *30*, 5194–5204.

(21) Wang, Y.; Dar, M. I.; Ono, L. K.; Zhang, T.; Kan, M.; Li, Y.; Zhang, L.; Wang, X.; Yang, Y.; Gao, X. et al. Thermodynamically Stabilized β-$CsPbI_3$–based Perovskite Solar Cells with Efficiencies $> 18\%$. *Science* **2019**, *365*, 591–595.

(22) Frost, J. M.; Butler, K. T.; Walsh, A. Molecular Ferroelectric Contributions to Anomalous Hysteresis in Hybrid Perovskite Solar Cells. *APL Mater.* **2014**, *2*, 081506.

(23) Frost, J. M.; Walsh, A. What is Moving in Hybrid Halide Perovskite Solar Cells? *Acc. Chem. Res.* **2016**, *49*, 528–535.

(24) Deretzis, I.; Di Mauro, B. N.; Alberti, A.; Pellegrino, G.; Smecca, E.; La Magna, A. Spontaneous Bidirectional Ordering of $CH_3NH_3^+$ in Lead Iodide Perovskites at Room Temperature: The Origins of the Tetragonal Phase. *Sci. Rep.* **2016**, *6*, 24443.

(25) Quarti, C.; Mosconi, E.; De Angelis, F. Structural and Electronic Properties of Organo-Halide Hybrid Perovskites from Ab Initio Molecular Dynamics. *Phys. Chem. Chem. Phys.* **2015**, *17*, 9394–9409.

(26) Mosconi, E.; Quarti, C.; Ivanovska, T.; Ruani, G.; De Angelis, F. Structural and Electronic Properties of Organo-Halide Lead Perovskites: A Combined IR-Spectroscopy and Ab Initio Molecular Dynamics Investigation. *Phys. Chem. Chem. Phys.* **2014**, *16*, 16137–16144.

(27) Carignano, M. A.; Kachmar, A.; Hutter, J. Thermal Effects on $CH_3NH_3PbI_3$ Perovskite from Ab Initio Molecular Dynamics Simulations. *J. Phys. Chem. C* **2015**, *119*, 8991–8997.

(28) Carignano, M. A.; Aravindh, S. A.; Roqan, I. S.; Even, J.; Katan, C. Critical Fluctuations and Anharmonicity in Lead Iodide Perovskites from Molecular Dynamics Supercell Simulations. *J. Phys. Chem. C* **2017**, *121*, 20729–20738.

(29) Selig, O.; Sadhanala, A.; Muller, C.; Lovrincic, R.; Chen, Z.; Rezus, Y. L.; Frost, J. M.; Jansen, T. L.; Bakulin, A. A. Organic Cation Rotation and Immobilization in Pure and Mixed Methylammonium Lead-Halide Perovskites. *J. Am. Chem. Soc.* **2017**, *139*, 4068–4074.

(30) Mattoni, A.; Filippetti, A.; Saba, M.; Delugas, P. Methylammonium Rotational Dynamics in Lead Halide Perovskite by Classical Molecular Dynamics: The Role of Temperature. *J. Phys. Chem. C* **2015**, *119*, 17421–17428.

(31) Mattoni, A.; Filippetti, A.; Saba, M. I.; Caddeo, C.; Delugas, P. Temperature Evolution of Methylammonium Trihalide Vibrations at the Atomic Scale. *J. Phys. Chem. Lett.* **2016**, *7*, 529–535.

(32) Deretzis, I.; La Magna, A. Exploring the Orthorhombic–Tetragonal Phase Transition in $CH_3NH_3PbI_3$: The Role of Atom Kinetics. *Nanoscale* **2017**, *9*, 5896–5903.

(33) Frost, J. M.; Butler, K. T.; Brivio, F.; Hendon, C. H.; Van Schilfgaarde, M.; Walsh, A. Atomistic Origins of High-Performance in Hybrid Halide Perovskite Solar Cells. *Nano Lett.* **2014**, *14*, 2584–2590.

(34) Kieslich, G.; Sun, S.; Cheetham, A. K. Solid-State Principles Applied to Organic–Inorganic Perovskites: New Tricks for an Old Dog. *Chem. Sci.* **2014**, *5*, 4712–4715.

(35) Flores-Livas, J. A.; Tomerini, D.; Amsler, M.; Boziki, A.; Rothlisberger, U.; Goedecker, S. Emergence of Hidden Phases of Methylammonium Lead Iodide ($CH_3NH_3PbI_3$) Upon Compression. *Phys. Rev. Mater.* **2018**, *2*, 085201.

(36) Sutton, R. J.; Filip, M. R.; Haghighirad, A. A.; Sakai, N.; Wenger, B.; Giustino, F.; Snaith, H. J. Cubic or Orthorhombic? Revealing the Crystal Structure of Metastable Black-Phase $CsPbI_3$ by Theory and Experiment. *ACS Energy Lett.* **2018**, *3*, 1787–1794.

(37) Car, R.; Parrinello, M. Unified Approach for Molecular Dynamics and Density-Functional Theory. *Phys. Rev. Lett.* **1985**, *55*, 2471.

(38) Deretzis, I.; Alberti, A.; Pellegrino, G.; Smecca, E.; Giannazzo, F.; Sakai, N.; Miyasaka, T.; La Magna, A. Atomistic Origins of $CH_3NH_3PbI_3$ Degradation to PbI_2 in Vacuum. *Appl. Phys. Lett.* **2015**, *106*, 131904.

(39) Röhm, H.; Leonhard, T.; Hoffmann, M. J.; Colsmann, A. Ferroelectric Domains in Methylammonium Lead Iodide Perovskite Thin-Films. *Energy Environ. Sci.* **2017**, *10*, 950–955.

(40) Rakita, Y.; Bar-Elli, O.; Meirzadeh, E.; Kaslasi, H.; Peleg, Y.; Hodes, G.; Lubomirsky, I.; Oron, D.; Ehre, D.; Cahen, D. Tetragonal $CH_3NH_3PbI_3$ is Ferroelectric. *Proc. Natl. Acad. Sci.* **2017**, *114*, E5504–E5512.

(41) Garten, L. M.; Moore, D. T.; Nanayakkara, S. U.; Dwaraknath, S.; Schulz, P.; Wands, J.; Rockett, A.; Newell, B.; Persson, K. A.; Trolier-McKinstry, S. et al. The Existence and Impact of Persistent Ferroelectric Domains in $MAPbI_3$. *Sci. Adv.* **2019**, *5*, eaas9311.

(42) Liu, S.; Zheng, F.; Koocher, N. Z.; Takenaka, H.; Wang, F.; Rappe, A. M. Ferroelectric Domain Wall Induced Band Gap Reduction and Charge Separation in Organometal Halide Perovskites. *J. Phys. Chem. Lett.* **2015**, *6*, 693–699.

(43) Giannozzi, P.; Baroni, S.; Bonini, N.; Calandra, M.; Car, R.; Cavazzoni, C.; Ceresoli, D.; Chiarotti, G. L.; Cococcioni, M.; Dabo, I. et al. QUANTUM ESPRESSO: A Modular and Open-Source Software Project for Quantum Simulations of Materials. *J. Phys. Condens. Matter* **2009**, *21*, 395502.

(44) Nosé, S. A Unified Formulation of the Constant Temperature Molecular Dynamics Methods. *J. Chem. Phys.* **1984**, *81*, 511–519.

(45) Perdew, J. P.; Burke, K.; Ernzerhof, M. Generalized Gradient Approximation Made Simple. *Phys. Rev. Lett.* **1996**, *77*, 3865.

(46) Vanderbilt, D. Soft Self-Consistent Pseudopotentials in a Generalized Eigenvalue Formalism. *Phys. Rev. B* **1990**, *41*, 7892.

(47) Verlet, L. Computer "Experiments" on Classical Fluids. I. Thermodynamical Properties of Lennard-Jones Molecules. *Phys. Rev.* **1967**, *159*, 98.

(48) Henkelman, G.; Uberuaga, B. P.; Jónsson, H. A Climbing Image Nudged Elastic Band Method for Finding Saddle Points and Minimum Energy Paths. *J. Chem. Phys.* **2000**, *113*, 9901–9904.

(49) Monkhorst, H. J.; Pack, J. D. Special Points for Brillouin-Zone Integrations. *Phys. Rev. B* **1976**, *13*, 5188.